Anal Bioanal Chem (2007) 387:83–89
DOI 10.1007/s00216-006-0789-3

ORIGINAL PAPER

Analysis of subcellular surface structure, function and dynamics

D. Anselmetti · N. Hansmeier · J. Kalinowski · J. Martini · T. Merkle · R. Palmisano · R. Ros · K. Schmied · A. Sischka · K. Toensing

Received: 8 May 2006 / Revised: 16 August 2006 / Accepted: 18 August 2006 / Published online: 3 November 2006

Abstract Analytics of single biological cells allows quantitative investigation from a structural, functional and dynamical point of view and opens novel possibilities to an unamplified subcellular analysis. In this article, we report on three different experimental methods and their applications to single cellular systems with a subcellular sensitivity down to the single molecule level. First, the subcellular surface structure of living bacteria (*Corynebacterium glutamicum*) was investigated with atomic force microscopy (AFM) at the resolution of individual surface layer (S-layer) proteins; discrimination of bacterial strains that lack the expression of hexagonally packed surface layer proteins was possible. Second, quantitative measurement of individual recognition events of membrane-bound receptors on living B-cells was achieved in single cell manipulation and probing experiments with optical tweezers (OT) force spectroscopy. And third, intracellular dynamics of translocating photoactivatable GFP in plant protoplasts (*Nicotiana tabacum BY-2*) was quantitatively monitored by two-photon laser scanning microscopy (2PLSM).

Keywords Atomic force microscopy · Optical tweezers · Two-photon laser scanning microscopy

D. Anselmetti (✉) · J. Martini · R. Ros · A. Sischka · K. Toensing
Experimental Biophysics and Applied Nanoscience,
Faculty of Physics, Bielefeld University,
Universitätsstraße 25,
33615 Bielefeld, Germany
e-mail: dario.anselmetti@physik.uni-bielefeld.de

N. Hansmeier · J. Kalinowski · T. Merkle · R. Palmisano · K. Schmied
Institute for Genome Research, Center of Biotechnology,
Bielefeld University,
Universitätsstraße 25,
33615 Bielefeld, Germany

Introduction

Single cell analysis at the subcellular level gives quantitative information from a structural, functional and dynamical point of view. The individual cell approach is inherently insensitive to ensemble-averaging effects and conceptually gives insights into cell-cycle-dependent states, different and inhomogeneous cellular responses to external stimuli, or the introduction of genomic and proteomic variabilities. The detection and analysis of single biomolecules and of minimal analyte quantities at the single cell level, requires sensitive and efficient techniques. Nanotechnology offers novel tools to detect, image, measure, analyze, steer and manipulate individual molecules and cells by atomic force microscopy (AFM) [1–6] and optical tweezers (OT) force spectroscopy [7–9] and allows more detailed insights into the physical mechanisms of specific interaction, binding kinetics and the interplay of genomic information and functional peculiarity at the single molecule or single cellular level. In recent years, a number of new single cell manipulation and analysis technologies like dielectric field cages [10], electron tomography [11], microgenomics and single cell gene expression analysis [12], single cell MALDI [13], laser microdissection and single cell catapulting [14] and single cell protein profiling in capillary electrophoresis [15] and microfluidics [16] have emerged. Some of these technologies rely on a subsequent amplification by (pre)concentration steps (like PCR), whereas some of them allow a direct investigation of the cellular systems at subcellular resolution.

In this article, three different methods, AFM, OT and two-photon laser scanning microscopy are presented. They can be applied to subcellular analysis with respect to structural, functional and dynamic information of living cells (bacteria and plant protoblasts) and exhibit a subcellular sensitivity down to the single molecule level.

Experimental

Atomic force microscope (AFM)

A commercial AFM instrument (Bioscope, Veeco, Santa Barbara) with standard non-contact silicon cantilever probes (BS-Tap 300Al, Budget Sensors, Sofia) was used under ambient laboratory conditions and operated in tapping mode. AFM surface topographs and phase signals were simultaneously recorded. Living gram-positive bacteria (*Corynebacterium glutamicum*, strain ATCC 14067 and strain ATCC 13032) were immobilized on hydrophilic glass by incubation and kept hydrated during the experiments. AFM raw data images have been processed only for background removal (flattening) by using the microscope manufacturer's image-processing software. More detailed preparative instructions for cell cultivation, transfection and handling have been published recently [17, 18].

Optical tweezers (OT)

A quantitative single-beam OT setup was integrated into an inverted optical microscope (Axiovert 100, Carl-Zeiss AG, Jena) with a 1-W, 1,064-nm Nd:YAG laser (Laser 2000, Wessling). With this setup, manipulation and steering of micron-sized objects like beads, colloids and cells can be achieved with a spatial resolution of 1 nm, a force sensitivity of 0.2 pN up to a maximum force of 380 pN. Details about the experimental setup have been published recently [9]. Living chicken DT40 B-cells were cultured in RPMI 1640 supplemented with 10% heat-inactivated fetal bovine serum, 1% heat-inactivated chicken serum, 10 units/mL penicillin, 10 μg/mL streptomycin and 2 mM L-glutamine at 37 °C and 5% CO_2. Before starting the experiments, the B-cells were washed twice and suspended in PBS buffer (136 mM NaCl, 2.7 mM KCl, 8.1 mM Na_2HPO_4 and 1.5 mM KH_2PO_4). For probing the membrane-bound B-cell receptors (BCR) biotinylated mouse anti-chicken IgM antibodies (msIgM) were used, that recognize the BCR (clone M-4; Southern Biotech, Birmingham) which were immobilized on streptavidin-coated polystyrol beads (3,180-nm diameter, binding capacity 60 pmol biotin/1 mg particle; Spherotec, Illinois).

Two-photon laser scanning microscope and photoactivatable GFP

In order to measure the intracellular protein dynamics of proteins that shuttle between the cell nucleus and the cytoplasm, we used a multifocal 2PLSM that consists of a mode-locked Tsunami Ti:Sa laser generating 100-fs laser pulses between 760 nm and 960 nm which is pumped by a Millenia X solid-state laser (both Spectra-Physics, Darmstadt), a TriM Scope multi focal scanning unit (LaVision BioTec, Bielefeld) and an inverted microscope (IX 71, Olympus, Hamburg). A more detailed instrumental description was recently published [19, 20]. As a photoactivatable protein we chose photoactivatable GFP (pa-GFP) [21] that allows spectral activation at $\lambda \approx 408$ nm in the nucleus, which induces a photoconversion resulting in an absorption maximum of the fluorescent protein at $\lambda \approx 488$ nm where it can be detected at an emission maximum of $\lambda \approx 517$ nm [22]. Transient co-transfection of the tobacco BY-2 protoplasts with pa-GFP and red-fluorescent protein (DsRed)-tagged prenylated Rab acceptor 1 (Pra1; At2g38360), a membrane protein that localises in speckles around the nuclear envelope, allows proper cell identification and visualisation before activation (via Pra1-DsRed fluorescence) and activation and protein dynamics monitoring (via pa-GFP fluorescence). Only molecules in the laser focus (activated by a burst of femtosecond 720- to 840-nm laser light pulses) will be photo-activated and hence will emit fluorescence at $\lambda \approx$ 520 nm when excited with light of $\lambda \approx 488$ nm by one-photon laser scanning microscopy (1PLSM) or $\lambda > 920$ nm by 2PLSM, respectively [23]. The use of near-infrared laser light for activation and detection is reasoned by the specific cross sections of pa-GFP, but it also provides the advantage of a higher penetration depth, negligible one-photon cross sections, and less potential for cellular damage and fluorescent background [24].

Results

Subcellular surface structure by AFM

Subcellular surface analysis of living cells like bacteria can be investigated at the nanometre scale by AFM. Bacterial strains ATCC 14067 and ATCC 13032 of *C. glutamicum* that are known to develop (ATCC 14067) and lack (ATCC 13032) an hexagonally ordered protein surface S-layer have been investigated in AFM experiments [18]. Under very humid and adequate imaging conditions these bacteria can be kept alive when immobilized on a surface under ambient laboratory conditions, remain in a hydrated state, and allow investigation with AFM. Figure 1a shows an AFM surface topography of several aggregated bacteria (ATCC 14067) in perspective representation. Already at this magnification features of the subcellular bacterium surface can be discerned. An irregular and disordered bacterial surface with protrusions on a length scale of ≈50 nm can be detected. It turned out that AFM imaging of these soft cellular systems is advantageous in the tapping mode of AFM operation, simultaneously recording topography and phase signal. We found that especially for resolving subcellular surface structures, AFM phase imaging renders

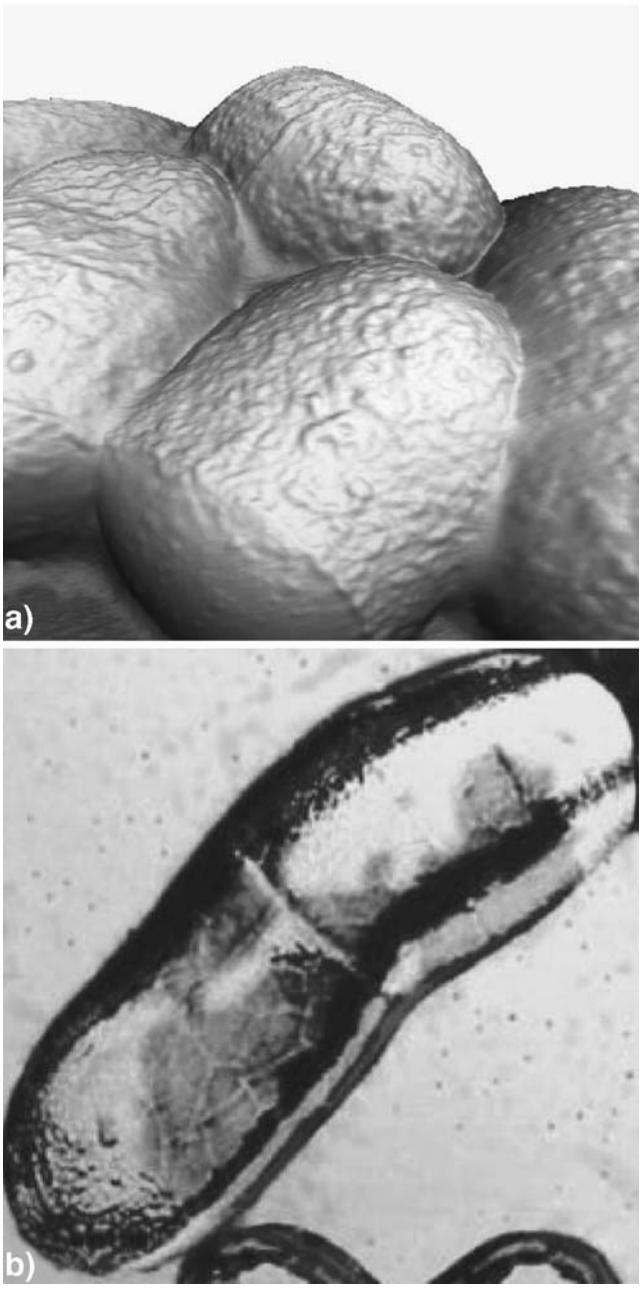

Fig. 1 AFM tapping mode images of living *C. glutamicum* ATCC 14067 cells with resolved subcellular surface structure (5-μm image). **a** AFM surface topograph exhibiting bacterial aggregates. **b** AFM phase image of isolated bacteria are visualized during cell divisional process in topview representation (3.9-μm image)

subtle nanometre-scale information. This finding is illustrated in Fig. 1b where the surface structure of an isolated bacterial cell (ATCC 14067) is shown in an AFM phase image. The resolved surface structure clearly indicates that this bacterium currently undergoes a cell division process. In order to identify and discriminate different bacterial strains we investigated the surface of the two bacterial strains ATCC 14067 and ATCC 13032 at higher resolution. On both bacterial systems we were able to resolve subcellular surface features that were irregular and disordered like in the AFM phase image of bacterial stain ATCC 13032 (Fig. 2a). Additionally on bacterial strain ATCC 14067, hexagonal surface structures with a periodicity of ≈15.4 nm (Fig. 2b,c) could be identified [18]. From earlier in vitro experiments, where bacterial S-layers were extracted and prepared on mica surfaces and identical regular array structures could be identified [17], and earlier in vivo experiments [25], an assignment of the measured subcellular array structures to the known 2D protein S-layer structure was possible. Moreover, the observation of the hexagonal S-layer array in Fig. 2b,c nicely corresponds to the fact that the bacterial strain ATCC 14067 is known to develop this protein surface motif. In contrast, on bacterial strain ATCC 13032, which lacks the relevant gene coding sequence for S-layer formation, we never observed subcellular surface features which could be associated with these surface protein arrays. Interestingly, these experiments were possible with bacterial strains that were not treated in order to remove the well-known polysaccharide surface layer (glycocalix) and nicely prove that AFM is able to resolve subcellular protein surfaces down to the level of individual protein monomers on single living cells, giving access to a direct test of genetic and protein variabilities.

Measuring individual membrane-bound receptors with photonic forces

In order to probe individual membrane-bound receptors in a functional way, single B-cells were immobilized on a surface (Fig. 3a). Alternatively, transfer and immobilisation of the B-cells to a micropipette held by low suction pressure is also feasible. For measuring individual membrane-bound B-cell receptors, a ms-IgM-functionalized microbead was trapped by the optical tweezers and carefully approached towards the B-cell with a constant velocity of 450 nm/s. The approach process stopped when a repulsive force of 5 pN was reached, which can directly be detected by the lateral displacement of the bead in the optical trap. Then, the bead was retracted from the cell without delay at a velocity of 1,000 nm/s. Upon recording the effective force during this approach–retract cycle (force–distance curves), the force interaction between msIgM and the cell-membrane-bound BCR could be measured, visible as an increasing attractive force during bead retraction. At a certain force the bond within the molecular complex dissociates which is indicated by the steep jump back to the baseline of zero force. A typical force–distance curve is presented in Fig. 4a (1). Characteristic dissociation forces in the range of 10 to 40 pN can be measured. It is worth noting that this dissociation process is of stochastic nature and statistically groups around a most probable value [26, 27]. The corresponding molecular

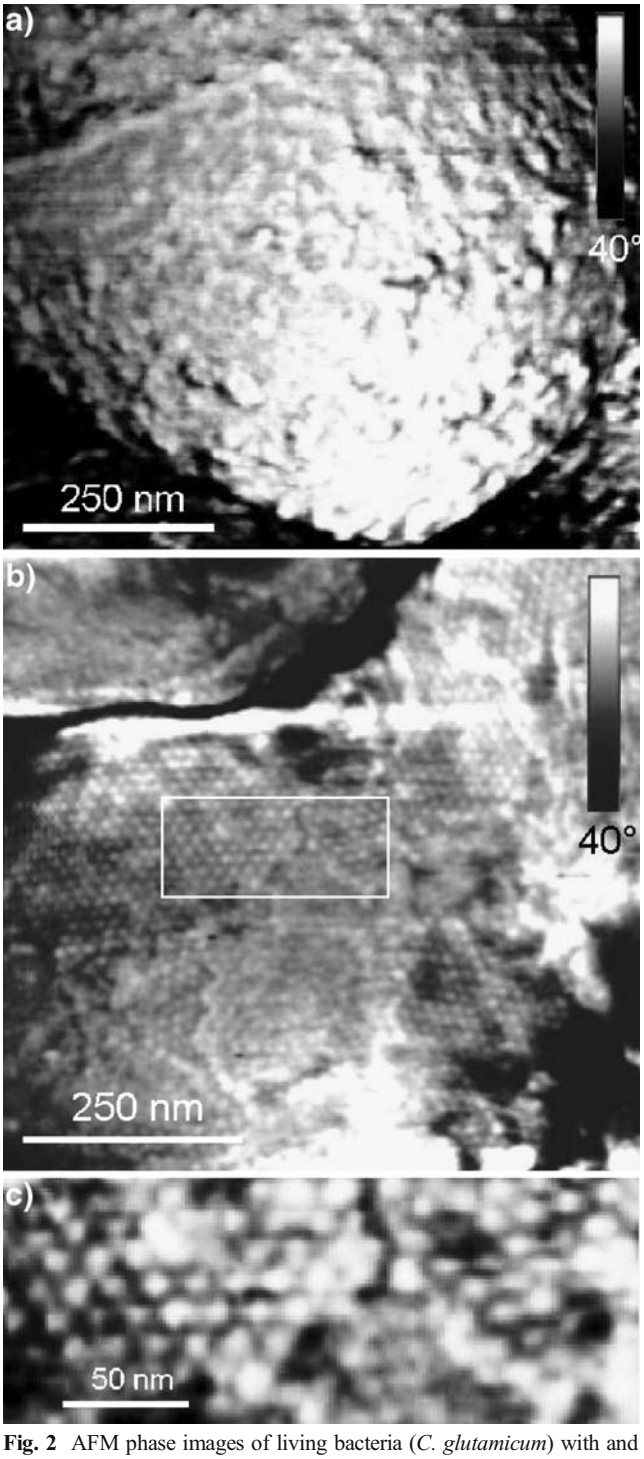

Fig. 2 AFM phase images of living bacteria (*C. glutamicum*) with and devoid of an ordered 2D protein S-layer structure. **a** Irregular subcellular surface structure on *C. glutamicum* strain ATCC 13032. **b** Hexagonally packed arrays of surface layer proteins on *C. glutamicum* strain ATCC 14067. **c** High-resolution AFM phase image showing the 18-nm lattice of the S-layer protein monomers on *C. glutamicum* strain ATCC 14067 (image corresponds to the region marked with a *box* in Fig. 2b)

loading rate of 45±5 pN/s, which indicates the force evolution on the complex, was calculated from the retraction velocity times the slope of the force–distance curve just before the rupture. About 30% of the force–

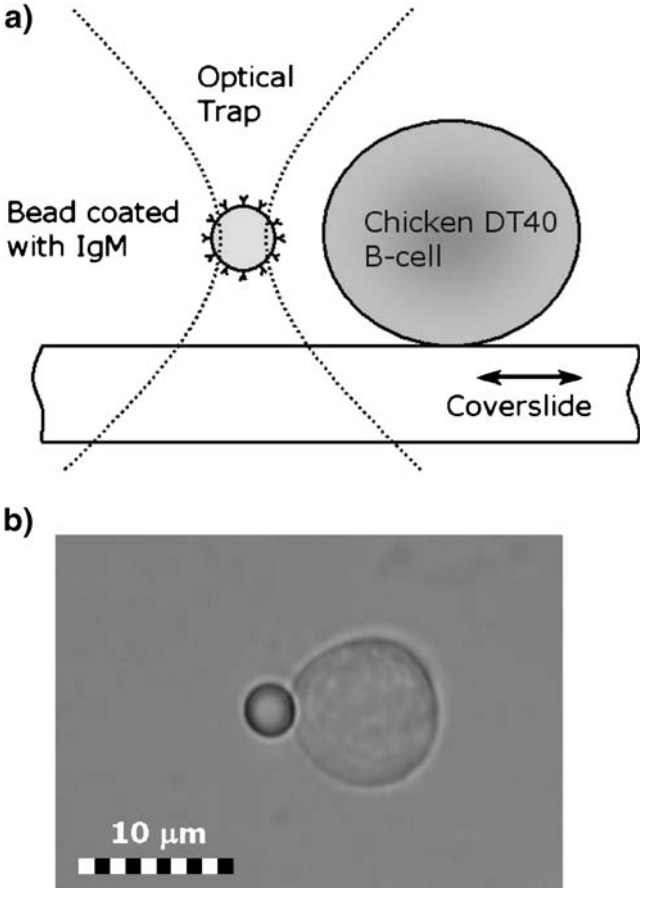

Fig. 3 **a** Schematic representation of single cell optical tweezer experiment. **b** Microscopic top view image of the B-cell, immobilized on a surface, and the antibody-coated bead that is steered by the optical trap

distance curves exhibit cell tether effects (Fig. 4a (2)) [28] associated with the binding of the msIgM to the highly viscous outer cell layer, causing an approximately constant force effect. This cell–tether phenomenon has already been observed and discussed in earlier receptor binding studies with AFM [29]. It is worth noting that in our study these binding force events were excluded from further data analysis. In this regard, Fig. 4b shows the histogram derived from tether-unaffected rupture force measurements. In order to exclude interactions which are due to non-specific background, only dissociation events above 6 pN were considered. In order to check for the specificity of the interaction, two control experiments have been conducted: 1) the competition with 15 pM free msIgM exhibited a strongly reduced overall activity, and 2) using beads coated only with streptavidin instead of msIgM no evidence of specific binding could be measured. An analysis of the force histogram in Fig. 4b exhibits individual peaks at ≈13, 21, 29 and 39 pN, indicating an integer number of interactions between msIgM and BCR. A Gaussian distribution to the first peak yields a single bond binding force of 12.5±0.8 pN for the given loading rate of 45 pN/s. The probability of observing single, double or multiple unbind-

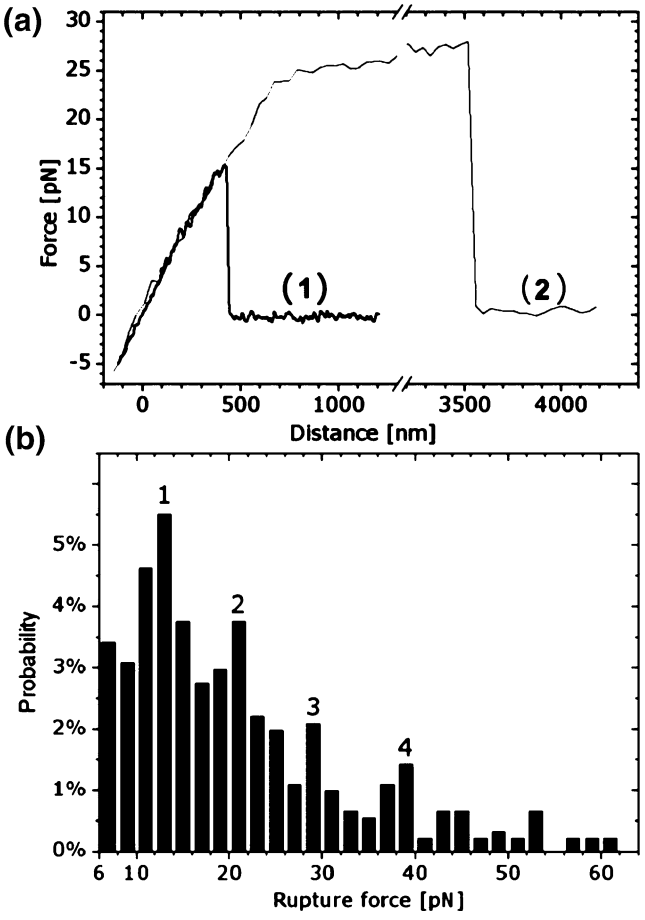

Fig. 4 **a** Typical force–distance curves obtained during retraction of the bead after forming a bond between the BCR and the msIgM showing distinct curve breakups associated with single bond ruptures. **b** Dissociation force histogram of the msIgM–BCR interaction (loading rate of 45±5 pN/s). Four peaks at 13, 21, 29 and 39 pN indicate an integer number of bonds forming between msIgM and the membrane-bound receptors

ing events is in good agreement with Poisson statistics, confirming the multiple rupturing characteristic of the investigated msIgM–BCR bonds and reflects the membrane receptor density of the probed cell within the area of contact. This experiment demonstrates the application of OT-based force spectroscopy for the specific measurement of membrane-bound B-cell receptors at the single molecule level. Generally, dynamic force spectroscopy experiments have the potential to measure the kinetics and thermodynamics of single membrane-bound receptors in vivo and to investigate structurally hierarchic or even more complex phenomena like receptor aggregation in biomembranes.

Intracellular protein dynamics

Intracellular protein dynamics of pa-GFP was recorded by local two-photon activation of pa-GFP in the cell nucleus and measuring the dynamics of its diffusion within the BY-2 protoplast from the nucleus into the cytoplasm by monitoring its temporal fluorescence propagation in the nucleus. In Fig. 5a,b two images out of a series of transmission–fluorescence images are shown, taken just at the start of photo-activation (26 s) and 974 s later. The nucleus of the protoplast is indicated by a dashed ellipse

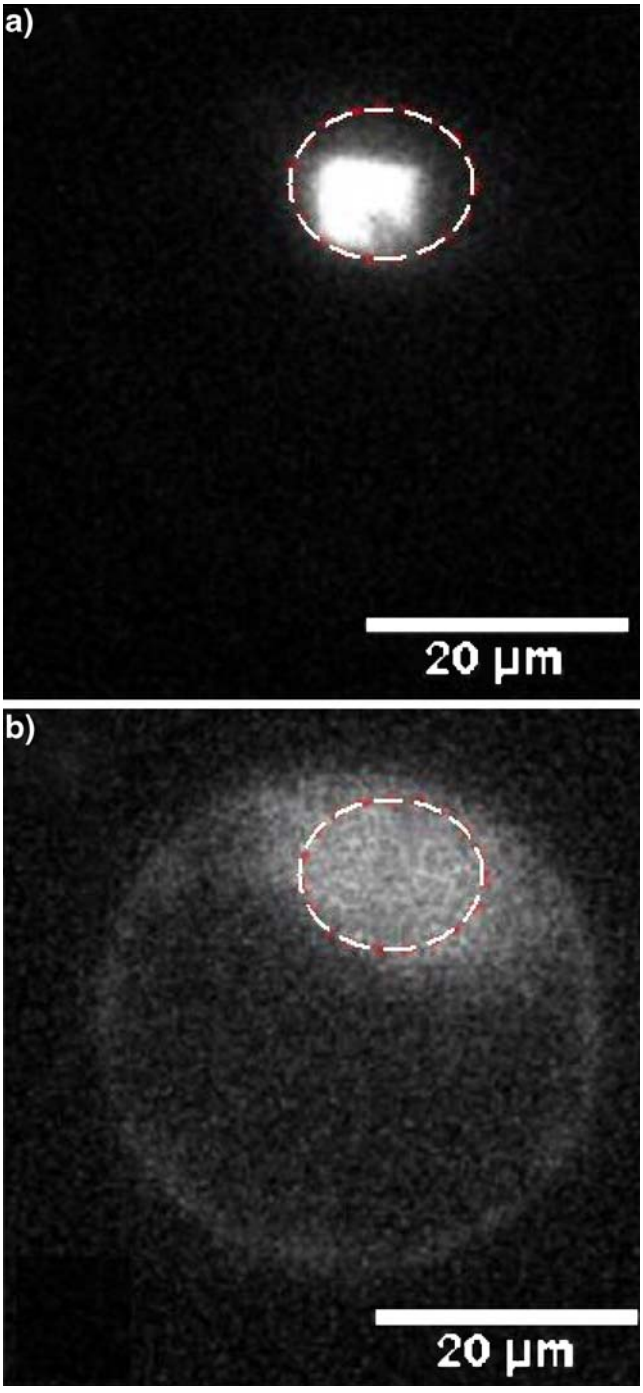

Fig. 5 Two 2PLSM transmission fluorescence images of pa-GFP protein dynamics of diffusional translocation in a live tobacco BY-2 protoplast. The cell nucleus is indicated by the *dashed line*. **a** During 2PLSM activation of pa-GFP in the nucleus (26 s). **b** After 1,000 s the pa-GFP fluorescence is leaking from the nucleus into the cytoplasm (for details see text)

that has been selected as a region of interest (ROI) for the subsequent temporal analysis of the fluorescence intensity decay. The decrease in fluorescence intensity within the ROI over time, directly displays the diffusion of pa-GFP from the nucleus into the cytoplasm as it gets accompanied by an increase of fluorescence there. It is noteworthy that the rectangular shape of strong fluorescence signal in Fig. 5a reflects the fact that pa-GFP activation was accomplished by scanning 4 parallel fs-laser foci over 3 s in the activation area of 7×8 μm^2 within the nucleus rather than point activation only. In order to quantify the kinetics of the decrease of pa-GFP fluorescence in the nucleus, we analysed the fluorescence intensity within the chosen ROI over the whole series of fluorescence images and plotted the results in Fig. 6. Directly after pa-GFP activation the ROI averaged fluorescence intensity is about 5 times greater compared to pre-activation measurements (data not shown), which essentially documents the great advantage of selectively "switching on" pa-GFP by light. The following decay of nuclear fluorescence intensity in time is due to the diffusion of activated pa-GFP fluorophores out of the nucleus into the cytoplasm. An analysis and fit of this temporal fluorescence decay cannot be explained properly by a single exponential function, indicating that photobleaching effects become important for long exposure times. This interpretation is supported by the fact that the fluorescence decay can be fitted in an excellent way by a bi-exponential decay, as indicated by the overlayed solid line in Fig. 6. According to this procedure, time constants for the two processes after pa-GFP photo-activation in the nucleus can be calculated, yielding 175 s and 2,100 s for pa-GFP translocation by diffusion and photobleaching, respectively. These experiments show that protein dynamics can quantitatively be monitored in living cells at subcellular resolution with a combination of local two-photon protein activation and subsequent monitoring of the intracellular fluorescence diffusion. We are confident that this new method gives access and insights into the quantitative real-time observation of intracellular dynamics of regulated processes like active nucleo-cytoplasmic partitioning of transcription factors.

Conclusion

A brief overview has been given of three different analytical methods—atomic force microscopy, optical tweezers and two-photon laser scanning microscopy—that allow analysis of individual living cells at subcellular or molecular resolution with respect of cell surface structure, membrane-bound receptor function and intracellular dynamics. In the future quantitative investigation of single biological cells at the subcellular level will give access to an unamplified single cell analysis without being subject to ensemble-averaging, cell-cycle or cell-population effects. Such techniques will have a broad spectrum of applications in systems nanobiology.

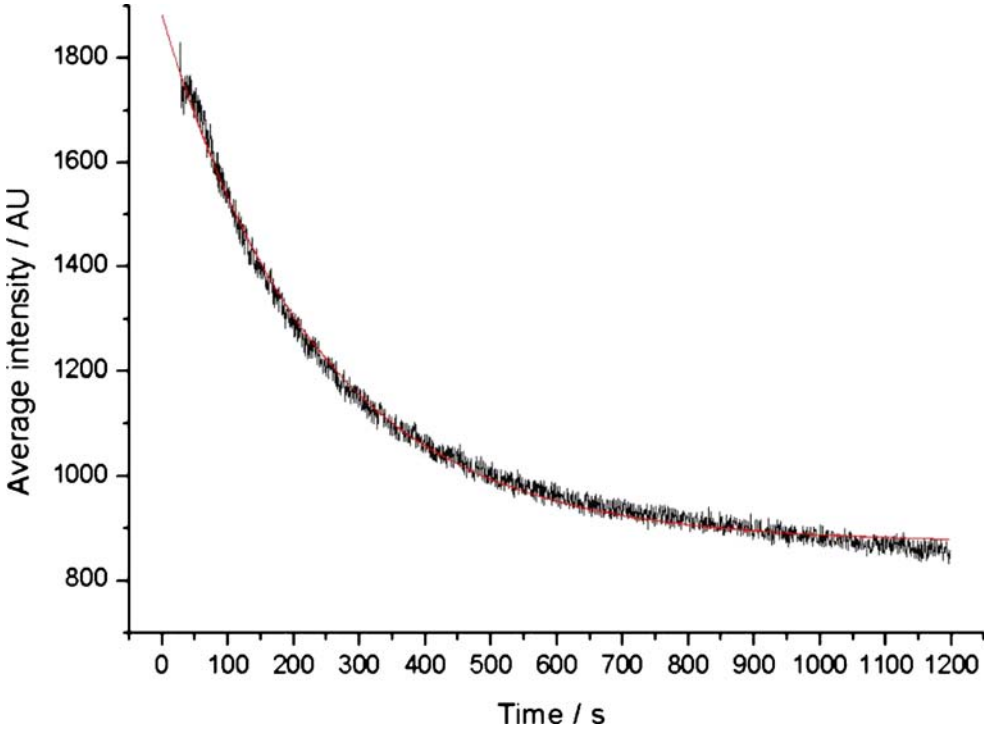

Fig. 6 Quantitative analysis of pa-GFP diffusion from the nucleus into the cytoplasm after its photo-activation in the nucleus. Bi-exponential fitting describes the overall decrease of fluorescence in very good approximation (*solid line*) yielding a diffusion time constant of 175 s (for details see text)

Acknowledgements Financial support from the Deutsche Forschungsgemeinschaft (DFG) within the Collaborative Research Project SFB 613-Physics of molecular recognition and single molecule processes in organic systems (D.A.), the Federal Ministry of Education and Research of Germany (BMBF) for the Research Project MEMO-Foundations of laser-based characterization of metabolism and morphology of biological tissue (D.A.) and from the DFG grants ME 1116/4–2 and BIZ 7/1–2 (T.M.) is gratefully acknowledged.

References

1. Binnig G, Quate CF, Gerber C (1986) Phys Rev Lett 56:930–933
2. Fritz J, Anselmetti D, Jarchow J, Fernandez-Busquets X (1997) J Struc Biol 119:165–171
3. Anselmetti D, Fritz J, Smith B, Fernandez-Busquets X (2000) Single Mol 1:53–58
4. Florin EL, Moy VT, Gaub HE (1994) Science 264:415–417
5. Bartels FW, Baumgarth B, Anselmetti D, Ros R, Becker A (2003) J Struct Biol 143:145–152
6. Eckel R, Wilking S D, Becker A, Sewald N, Ros R, Anselmetti D (2005) Angew Chem Int Ed 44:3921–3924
7. Ashkin A (1997) Proc Natl Acad Sci USA 94:4853–4860
8. Bustamante C, Bryant Z, Smith SB (2003) Nature 421:423–427
9. Sischka A, Eckel R, Toensing K, Ros R, Anselmetti D (2003) Rev Sci Instrum 74:4827–4831
10. Reichle C, Sparbier K, Müller T, Schnelle T, Walden P, Fuhr G (2001) Electrophoresis 22:272–282
11. Baumeister W, Grimm R, Walz J (1999) Trends Cell Biology 9:81–85
12. Levsky JM, Shenoy SM, Pezo RC, Singer RH (2002) Science 297:836–840
13. Li L, Garden RW, Sweedler JV (2000) Trends Biotechnol 18: 151–160
14. Thalhammer S, Lahr G, Clement-Sengewald A, Heckl WM, Burgemeister R, Schütze K (2003) Laser Physics 13:681–691
15. Hu S, Zhang L, Krylov S, Dovichi NJ (2003) Anal Chem 75:3495–3501
16. Ros A, Hellmich W, Regtmeier J, Duong TT, Anselmetti D (2006) Electrophoresis 27:2651–2658
17. Hansmeier N, Bartels FW, Ros R, Anselmetti D, Tauch A, Pühler A, Kalinowski J (2004) J Biotechnology 112:177–193
18. Hansmeier N, Albersmeier A, Tauch A, Damberg T, Ros R, Anselmetti D, Pühler A, Kalinowski J (2006) Microbiology 152:923–935
19. Martini J, Toensing K, Dickob M, Anselmetti D (2005) Proc SPIE 5860:16–21
20. Martini J, Toensing K, Dickob M, Schade R, Liefeith K, Anselmetti D (2006) Proc SPIE 6089:274–282
21. Patterson GH, Lippincott-Schwartz J (2002) Science 297:1873–1877
22. Patterson GH, Lippincott-Schwartz J (2004) Methods 32:445–450
23. Schneider M, Barozzi S, Testa I, Faretta M, Diaspro A (2005) Biophys J 89:1346–1352
24. Zipfel WR, Williams RM, Webb WW (2003) Nature Biotech 21:1369–1377
25. Dufrene YF (2001) Micron 32:153–165
26. Evans E (1999) Faraday Discuss 111:1–16
27. Raible M, Evstigneev M, Bartels FW, Eckel R, Nguyen-Duong N, Merkel R, Ros R, Anselmetti D, Reimann R (2006) Biophys J 90:3851–3864
28. Dai J, Sheetz MP (1999) Biophys J 77:3363–3370
29. Bustanji Y, Arciola CR, Conti M, Mandello E, Montanaro L, Samori B (2003) Proc Natl Acad Sci (USA) 100:13292–13297